Title
Optical Emission Spectroscopy and Gas Kinetics of Picosecond Laser-Induced Chlorine Dissociation for Atomic Layer Etching of Silicon.

Journal
The Journal of Physical Chemistry C, 129(5)

ISSN
1932-7447

Authors
Li, Runxuan
Eliceiri, Matthew
Li, Jingang
et al.

Publication Date
2025-02-06

DOI
10.1021/acs.jpcc.4c07330

Peer reviewed

THE JOURNAL OF PHYSICAL CHEMISTRY C
A JOURNAL OF THE AMERICAN CHEMICAL SOCIETY

pubs.acs.org/JPCC
Article

Optical Emission Spectroscopy and Gas Kinetics of Picosecond Laser-Induced Chlorine Dissociation for Atomic Layer Etching of Silicon

Runxuan Li, Matthew H. Eliceiri, Jingang Li, Vasileios Korakis, Rundi Yang, Yoonsoo Rho, Brian W. Blankenship, and Costas P. Grigoropoulos*

Cite This: J. Phys. Chem. C 2025, 129, 2460−2466
Read Online

ABSTRACT: The continuing developments in semiconductor device technologies have prompted the need for advanced nanoscale processing techniques. Laser chemical processing offers significant advantages, including spatial selectivity, high localization, minimal material damage, and fast operation. Pulsed laser-induced dissociation of gas species serves as an essential process step, contributing to doping, etching, and other chemical modifications of semiconductor materials. However, the mechanisms behind the laser−gas interactions and subsequent surface modifications remain elusive. Here, we demonstrate ultraviolet picosecond laser-induced atomic layer etching of silicon in a gaseous chlorine environment, achieving self-limited etching with a precision of 0.93 nm/cycle. Through *in situ* optical emission spectroscopy, we elucidate the transition energy states of laser-excited products during chlorination. Complementing our experimental findings, we perform numerical modeling that reveals the complex spatiotemporal dynamics of chlorine species, encompassing their generation, recombination, diffusion, and transient surface reaction with the silicon substrate. Our study demonstrates optical diagnostics of laser-induced chlorination in atomic layer etching, which can provide valuable insights into ultrafine chemical nanostructuring of semiconductor materials.

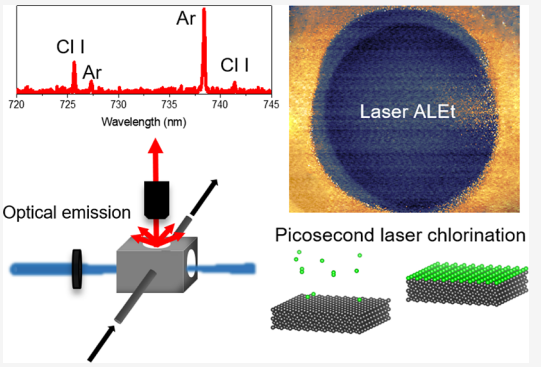

1. INTRODUCTION

The continuing miniaturization of semiconductor devices drives a need for new and advanced fabrication techniques to create fine feature sizes with high precision.[1] Atomic layer etching (ALEt) is a key technology in this progression, offering atomic-level precision and enabling self-limited removal of one or a few layers of material.[2] A two-step procedure differentiates such digital etching from its continuous counterpart: first, a reactive layer is formed, and subsequent incident energy deposition takes off only the modified layer.[3] Considering silicon as an example, this process involves the adsorption of Cl atoms on the surface forming $SiCl_x$ ($x \leq 4$)[4] and subsequent removal of this layer by either ion bombardment, thermal desorption, or laser irradiation. The conventional method for introducing chlorination typically involves an inductively coupled plasma source to provide the energy for chlorine dissociation. While plasma-assisted ALEt is highly scalable and has been applied to a variety of materials, the process involves complex equipment and demands sophisticated process control.[5] Furthermore, it is prone to dark etching in the reaction step and high-mass ion damage in the etching step. This issue limits the level of carrier concentration doping in sensitive materials such as ultrathin films and two-dimensional (2D) layers.[6] Consequently, this work demonstrates the effectiveness of laser-assisted ALEt, where the high-energy plasma source in the reaction or etching step is replaced with a laser. Compared to plasma ALEt, laser-assisted ALEt requires lower vacuum conditions and offers faster processing rates, higher spatial resolution, and exhibits less variation in the processing parameters.[7] Leaning on these advantages, laser-assisted ALEt has been applied to Si,[7,8] III−V semiconductors,[9,10] and 2D materials.[11,12]

Laser chemical processing has been a widely studied topic on doping, etching, and ion implantation of materials.[13,14] In such processes, a continuous wave or pulsed laser irradiates the material specimen under the flow of a reactive gas. Optically/thermally excited atoms or molecules then interact with the surface of the sample *via* physisorption or chemisorption. For instance, phosphorus doping in transition metal dichalcogenides was achieved by continuous wave laser irradiation in a phosphine environment.[15] Continuous etching of silicon was

Received: October 28, 2024
Revised: January 10, 2025
Accepted: January 13, 2025
Published: January 22, 2025

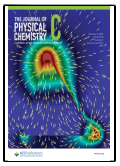

https://doi.org/10.1021/acs.jpcc.4c07330
J. Phys. Chem. C 2025, 129, 2460−2466

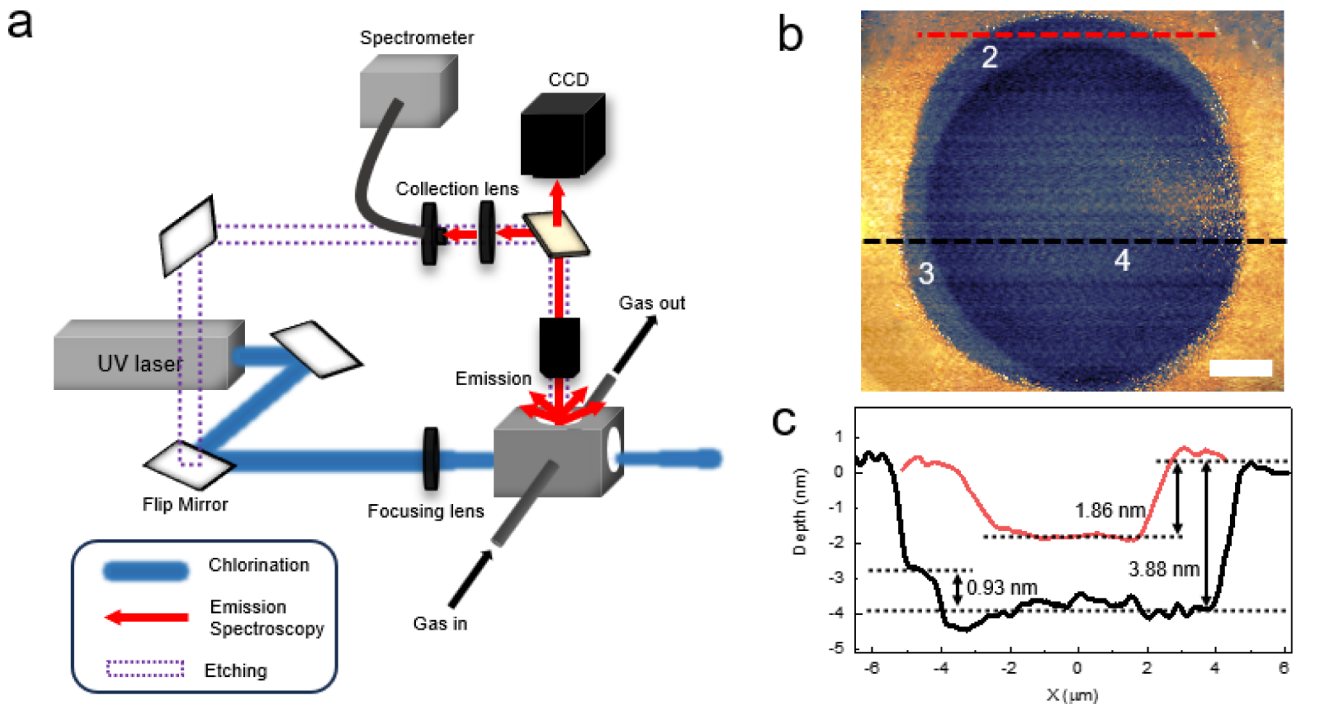

Figure 1. (a) Schematic of picosecond-induced chlorination, *in situ* optical emission spectroscopy, and subsequent etching. (b) AFM topography of overlapping laser-assisted ALEt processed spots. Scale bar is 2 μm. (c) Line traces of the etch pit showing the etching of 2, 3, and 4 cycles.

also realized by ultraviolet (UV) irradiation in a chlorine atmosphere.[16] These methods are effective, yet not prohibitively complicated to implement. However, their ability to decouple surface adsorption from the subsequent target modification is impaired since all process steps are triggered by a single irradiation event. Additionally, the development of more versatile, finely tuned, and better-controlled laser chemical processing would benefit from detailed analysis of the interaction of the laser with the processing gas. While optical diagnostics methods have been widely used in characterizing laser-solid interactions,[17−19] less attention has been given to laser−gas interactions in laser-assisted ALEt.

In this work, we report the laser-assisted ALEt of silicon by using a single laser source. A 355 nm picosecond laser is first directed parallel to the silicon surface to dissociate Cl_2 gas for surface chlorination and then delivered in the normal direction to induce transient heating for $SiCl_x$ desorption. In our previous work, we used a 266 nm ns laser for the chlorination of silicon and demonstrated the self-limiting characteristic with respect to time in surface passivation and laser fluence in the etching depth. While changing this laser affects the photodissociation and surface adsorption time, the self-limiting behavior of the process remains intact.[7] The 355 nm laser was chosen to match the absorption cross-section of chlorine molecules and provide good thermal confinement due to the shallow penetration depth in silicon. Compared to conventional plasma chlorination, the atoms produced by photodissociation have much lower kinetic energy, thereby eliminating unwanted dark etching of the sample.[20] We further investigate the *in situ* optical emission spectrum of excited chlorine atoms during laser-induced dissociation and reveal the transition states of Cl atoms due to ultrafast laser excitation. The time-resolved Cl_2 dissociation and atom adsorption onto the underlying silicon substrate are analyzed by a numerical model considering the three different time scales that correspond to dissociation (picoseconds), diffusion (microseconds), and adsorption (milliseconds to seconds). Our results provide a methodology to analyze the density of diatomic gas reactants under laser dissociation and their reactions with semiconductor interfaces and devices.

2. METHODS

2.1. Experiment Setup. The laser-assisted ALEt setup is equipped with a vacuum chamber having optical windows on four sides and gas delivery tubes on two sides.[7] The flow of Cl_2/Ar is set to 100 sccm, and the pressure in the chamber is regulated by a throttle valve. The vacuum chamber is mounted on a precision *x*-*y*-*z* mechanical stage. The laser source is a 355 nm ps laser (Passat Compiler), which can operate at a maximum rate of 400 Hz and emit 160 μJ per pulse. The full width at half-maximum (fwhm) pulse length of the laser is 6 ps. The laser beam passes through a polarizing beam splitter and half-wave plate (Thorlabs) for power modulation. A flip mirror (Thorlabs) is installed to direct the laser either in the parallel or the normal to the sample direction. During the chlorination (parallel irradiation) process, the laser is focused to a beam waist of 100 μm located 0.5 mm above and parallel to the silicon chip, while a spectrometer (Avantes) with 0.14−0.18 nm spectral resolution collects the optical emission signal *in situ* with a gate width of 10 μs. The atomic force microscope (AFM) data were acquired with a Molecular Vista VistaScope instrument.

2.2. Numerical Simulations. Simulation of the chlorine atomic density with respect to space and time is conducted using the finite difference method in MATLAB, assuming radial symmetry. The numerical solver accounts for an area of 2 mm × 2 mm, where the laser is focused at the origin to a beam waist of 100 μm. The numerical simulation is implemented on a uniform grid, with grid spacing d*x* and d*y* of 5 μm chosen to resolve the critical features of the laser dopant generation and diffusion processes. The time discretization is performed using an explicit variable-time stepping scheme with the boundary condition

https://doi.org/10.1021/acs.jpcc.4c07330
J. Phys. Chem. C 2025, 129, 2460−2466

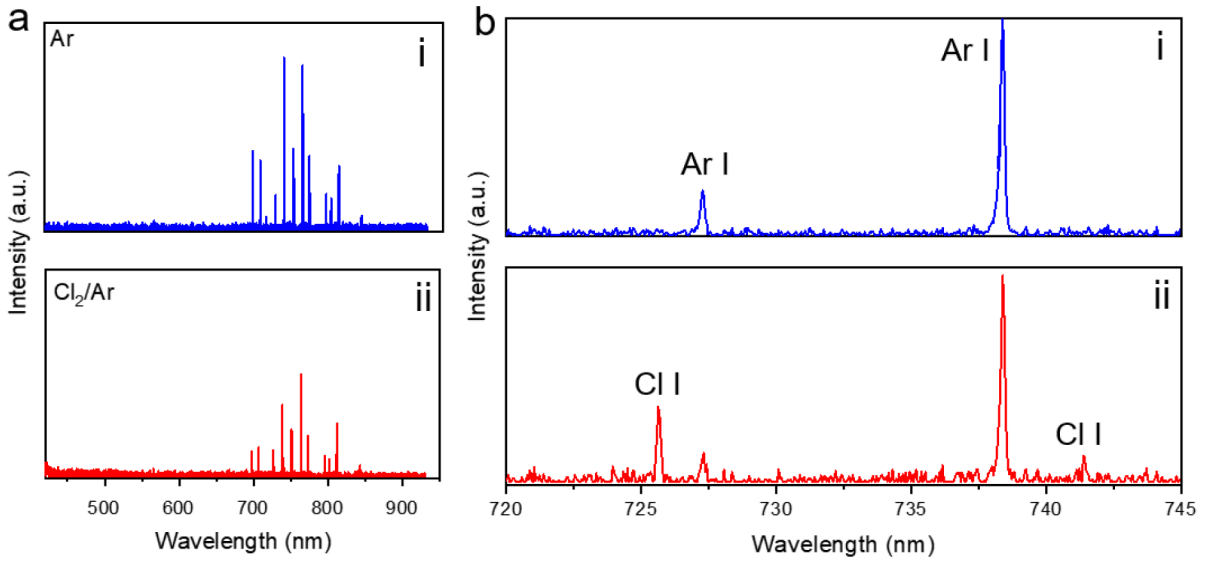

Figure 2. (a) 400−1000 nm spectrum excited by single pulse picosecond laser excitation of (i) Ar and (ii) Cl_2/Ar mixture. (b) 720−745 nm spectrum of (i) Ar and (ii) Cl atomic emission.

applied at each time step to update the concentration profile. To ensure accuracy in the picosecond laser excitation regime, a time step, Δt, of 1 ps is chosen to capture the transient characteristic of the intrapulse generation effect. Accounting for numerical stability and saving computational time, a Δt of 1 ns is used in the diffusion and recombination steps.

3. RESULTS AND DISCUSSION

3.1. Laser-Assisted ALEt. The laser-assisted ALEt setup is shown in Figure 1a. A heavily boron-doped <111> silicon chip is immersed in buffered hydrofluoric acid to remove native oxide and then placed inside a vacuum chamber. Cl_2/Ar is flowed to fill the chamber with a constant pressure of 40 Torr (5332.9 Pa), with a partial pressure of 2 Torr (266.645 Pa) for Cl_2. Once this constant pressure is attained, the picosecond laser applies pulses at 400 Hz for 30 s to chlorinate the silicon sample. The laser-induced dissociation and atomic transitions of chlorine atoms are monitored by *in situ* optical emission spectroscopy (Figure 1a). After the chlorination step, we reoriented the optical path of the picosecond laser normal to the silicon chip with a fluence of 0.2 J cm^{-2} (2×10^3 J m^{-2}) to remove ∼1 nm of the silicon. Figure 1b shows the AFM of the etch pits after 4 cycles of the etching process on an overlapped area. The profile of the irradiated spot is highly uniform and shows a clear digital self-limited behavior wherein the height difference between each cycle is 0.93 nm, while 4 cumulative cycles yield a depth of 3.88 nm (Figure 1c). The presence of overlapping etching pits corresponding to 2−4 cumulative cycles evinces the cyclic nature as well as the unintrusive Cl reactions that take place in the reaction step. Etch pits with 1 and 2 etching cycles with different processing fluences can be found in Figure S1.

We found that the Gaussian profile of the laser did not affect the uniformity of the etch pits, indicating that the self-limited etching mechanism differs from ablative material removal or continuous etching. This shows that the laser-assisted ALEt process can produce high-precision patterning and selectively etch silicon without photolithographic pattern transfer. The UV penetration depth of silicon is around 10 nm, strongly confining the absorption area, which minimizes thermal damage to the sample. Furthermore, compared to argon ion bombardment in plasma ALEt, this process is essentially instantaneous and does not depend on the processing time.

3.2. Optical Emission Spectroscopy. Chlorine molecules absorb light in the range of ∼190−500 nm with the absorption cross-section maximum situated at 335 nm, while the full width at half-maximum of the absorption band is around 60 nm.[21] In our experiment, chlorine molecules dissociate by a single photon absorption process at 355 nm with an atomic quantum yield of 2.[22,23] The dissociated chlorine atoms each with an unpaired electron are highly reactive and bond to pristine and defective sites of silicon to form bonds, reducing the binding energy of the underlying layers.[24] The dissociation product channels to the ground state Cl ($^2P_{3/2}$) and the excited state Cl ($^2P_{1/2}$) due to spin−orbit coupling.[25] Johnsen et al. performed a quantum mechanical simulation of the photodissociation process and identified the main dissociation channel for 355 nm irradiation, yielding atomic products in the Cl ($^2P_{3/2}$) state.[26] To understand the mechanism of chlorination in the ALEt experiment, we performed the aforementioned gas dissociation while *in situ* monitoring under Cl_2/Ar and Ar environments. The spectral lines between 700 and 800 nm show groups of atomic emission lines from both excited Ar atoms and Cl atoms (Figure 2a). Two strong lines at the wavelengths of 725.67 and 741.41 nm are observed, corresponding to the chlorine atomic transitions from the 4S° and 2P° states to the 4P state (Figure 2b), thus indicating the presence of photofragmented chlorine atoms which validates the mechanism of chlorine-induced etching. Since the 355 nm photodissociation process generates atoms in the ground state, the two elevated energy levels 10.57 and 10.60 eV above the ground state are due to atomic absorption of three photons after dissociation and during the trailing part of the laser pulse.[27] We further measure the lifetime of the 725.67 nm energy transition by applying a 725 nm notch filter to an avalanche photodiode, where an energy transition lifetime of ∼5 ns can be detected (Figure S2b). The recombination chemiluminescence of two chlorine atoms from third body quenching effects typically emits radiation at 844.1 nm.[28] However, no chemiluminescence (844.1 nm) was observed, which can be attributed to the small quantum yield of this reaction in our low-pressure setup.[29] Notably, lines with higher

https://doi.org/10.1021/acs.jpcc.4c07330
J. Phys. Chem. C 2025, 129, 2460−2466

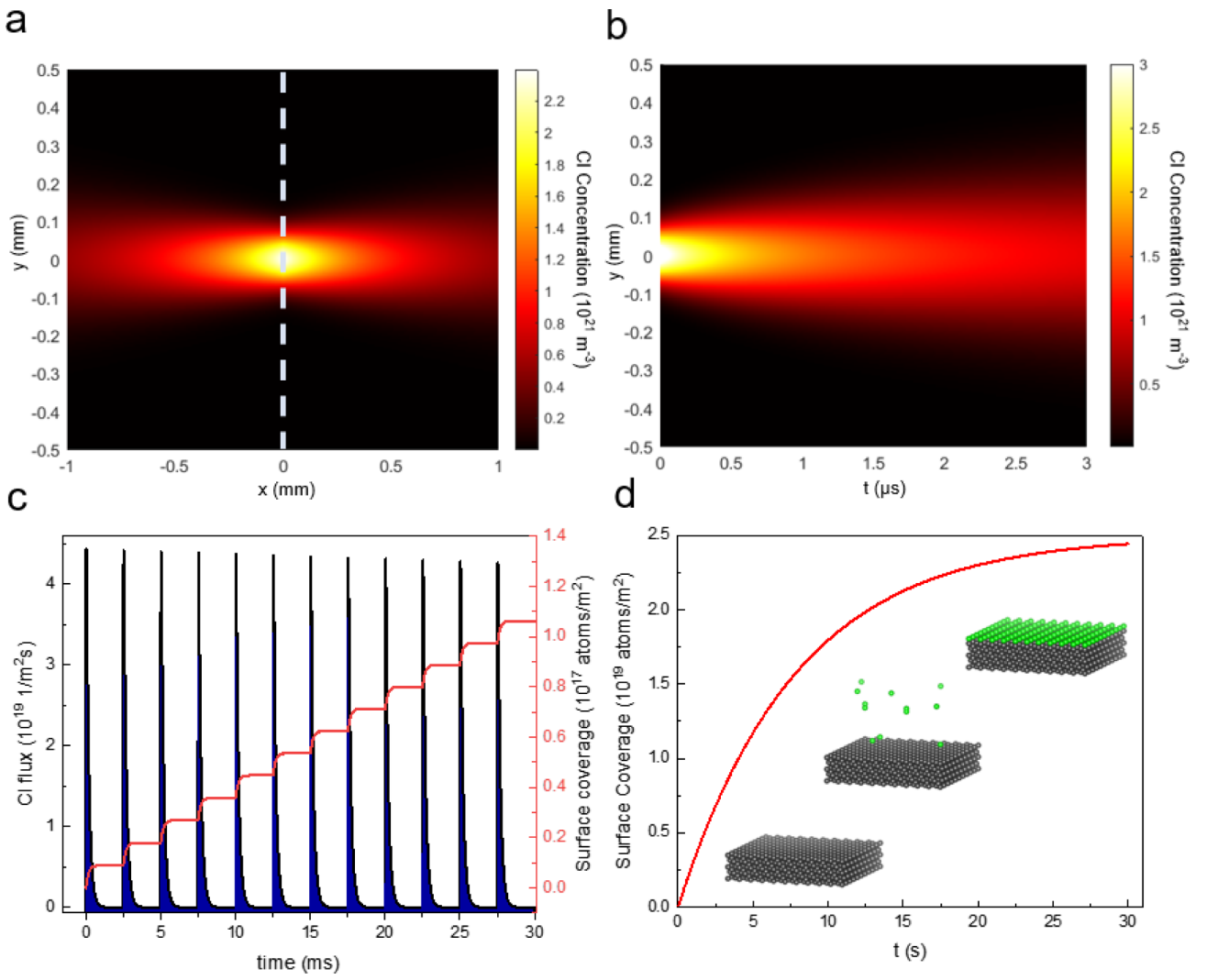

Figure 3. (a) Atomic chlorine concentration at 3 ps, when laser is at peak intensity. (b) Time-dependent dynamics of the chlorine atoms from 0 to 3 μs across vertical positions from −0.5 mm to 0.5 mm. (c) Chlorine atomic flux at the silicon boundary 0.5 mm below the laser focus spot with the laser operated at 400 Hz repetition rate. Vertical axis on the right is the integrated flux showing the adsorbed Cl atoms over 30 ms. (d) Surface coverage of the Si surface as a function of time when the laser is operated at 400 Hz.

intensity typically found in a chlorine plasma corresponding to the first-degree ionized Cl atoms at (479.5 nm, 481.0 nm) were not present in the laser photodissociation.[30,31] This proves that laser-assisted chlorination is an energy-efficient and charged species-free method, where undesired effects such as ion spallation damage and premature etching can be avoided.[32] The intensity of the two Cl atomic lines provides a direct, real-time diagnostic of the chlorine dissociation process, as they are strongly correlated with Cl atomic density. Due to equipment limitations, the maximum laser power is used, and the intensity of atomic lines is increasingly vague with lowered power. The microsecond time-resolved integrated emission intensity spikes when the pulse arrives and quickly decays, indicating the optimum operating condition of our diagnostic platform (Figure S2a). The *ex situ* AFM data confirmed that under argon flow followed by vertical irradiation, no etching effect was observed (Figure S1a,b), while processing in a chlorine atmosphere caused the removal of 0.93 nm per cycle (Figure S1c−e).

3.3. Photodissociated Chlorine Atom Kinetics. To investigate factors influencing the laser-induced chlorine dissociation and adsorption to the silicon sample, we developed a mathematical model to characterize the chlorination process (see Section 2 and Figure S3 for more details). The dynamics of chlorine gas within this simulation domain are described by the diffusion equation coupled with reaction kinetics.[33] The concentration of atomic chlorine (N_{Cl}) evolves over time due to dissociation from the UV picosecond laser, diffusion, and recombination. In order to investigate the efficiency of the laser-assisted chlorination, the following differential equation is used:[33]

$$\frac{\partial N_{Cl}(x, y, t)}{\partial t} = 2\sigma N_{Cl_2} I(x, y, t)\frac{\lambda}{hc} - 2k_{Cl_2} N_{Cl}^2(x, y, t) N_{Cl_2} - 2k_{Ar} N_{Cl}^2(x, y, t) N_{Ar} + D\nabla^2 N_{Cl}(x, y, t) \quad (1)$$

where the first term on the right-hand side denotes the generation of atoms from the picosecond laser and σ is the absorption cross-section of Cl_2 corresponding to the experimental conditions provided in Table S1.[21] Only single-photon absorption is accounted for due to chlorine molecules' large

https://doi.org/10.1021/acs.jpcc.4c07330
J. Phys. Chem. C 2025, 129, 2460−2466

absorption cross-section at 355 nm, and the absorption of one photon will produce two chlorine atoms.[22,23] Due to the adiabatic nature of photodissociation at 355 nm, the temperature effect on the collision and kinetic energy loss is not considered.[22] The second and third terms indicate the recombination due to the third body quenching reaction with k_{Cl_2} and k_{Ar} being the rate constants for reaction with Cl_2 and Ar.[29] The fourth term quantifies the diffusion of gas phase atoms using Fick's law. Advection is ignored because the chamber is kept at constant pressure, and minimal flow evolves under the experimental conditions. The parameters in the simulation and their detailed descriptions are presented in Table S1. The boundary condition is defined as variable flux derived from the interaction between the atomic chlorine and the vacuum chamber surface:[34]

$$J = \frac{1}{4}\eta\bar{v}N_{Cl} \tag{2}$$

Here, η represents the sticking coefficient of chlorine atoms at the chamber surface.[16] This atomic flux is also calculated by (2) for chlorine−silicon interaction with the sticking coefficient following the Langmuir adsorption model with $\bar{v}$ being the mean thermal velocity of chlorine atoms.[34]

The spatial distribution of chlorine atomic density calculated by (1) when the first laser pulse intensity is at its maximum (3 ps after onset) is illustrated in Figure 3a. The spatial distribution of the laser irradiance at the same time instance is shown in Figure S4a, and the Gaussian temporal profile of the picosecond pulse is provided in Figure S4b. As the laser beam travels along the horizontal direction, the center of the focal zone attains an atomic concentration density reaching 10^{21} m^{-3}, corresponding to 1% of the maximum permissible dissociated chlorine density at the experimental pressure conditions. This initial density is 2 magnitudes higher than that produced by a high-density plasma reactor.[35] The almost symmetric density distribution on the left and right of the focus is attributed to the long extinction depth relative to the simulation region along the laser propagation direction. With the parameters in Table S1, we estimate the fraction of Cl_2 dissociated at the laser focus is approximately 15% after a single irradiation event. As the first pulse finishes, the atomic chlorine diffuses, driven by the laser-induced concentration gradient. Figure 3b shows the transient atomic concentration in the microsecond regime across the vertical axis, marked by the dashed lines in Figure 3a. Due to the sluggish diffusion of Cl atoms, this process takes ∼0.1 s to reach a steady-state distribution. However, on the silicon surface situated −0.5 mm below the focal axis of the laser beam, the chlorine atom flux rapidly increases to a high level (∼10^{19} m^{-2} s^{-1}) and decays until the subsequent pulse arrives. The atomic spatial concentration distribution and flux are dynamically stable due to pronounced third-body recombination at higher Cl densities (Figure 3c). This indicates that laser-chlorination under the present experimental conditions is a linear process when the sample surface is not saturated. The flux gradually decreases as surface coverage increases on the silicon substrate and the adsorbate's surface coverage reaches an asymptote of 2.5 × 10^{19} m^{-2} or 1 monolayer at ∼30 s,[36] matching our experimental condition for an effective chlorination cycle time (Figure 3d). To accelerate the surface saturation, various parameters in the laser ALEt can be further optimized, such as using a higher repetition rate laser for the flux to be maintained at an elevated level. Keeping the sample closer to the focal center can induce a larger concentration gradient, thereby enhancing the chlorination efficiency.

4. CONCLUSION

In conclusion, we performed ALEt of silicon as a model system by a two-step process using a UV picosecond laser to induce chlorination and etching. The first step is monitored by optical emission spectroscopy, verifying chlorine atom generation through the laser dissociation process and revealing the energy states of the laser-excited Cl atoms. The laser-induced dissociation is then further investigated by a numerical model to determine the transient kinetics and surface interactions. Using this model, the transient three-dimensional distribution of the concentration is resolved. The calculated saturation time matches the experimental observations, rendering our work a robust and efficient procedure for characterizing laser-assisted ALEt. Future work incorporating laser sources offering higher fluence and larger beam cross-sections would potentially assist in measuring recombination luminescence and other energy levels with optical emission spectroscopy. A confocal variant of our spectroscopic methods,[37,38] could be applied to spatially resolve halogen dissociation processes. By correlating the *in situ* emission with the chlorine atomic density derived by the developed numerical model, the surface coverage could potentially be evaluated online during any ALEt process, thereby improving the process yield of ALEt on nanostructures[39,40] and devices.[41,42]

■ ASSOCIATED CONTENT

Supporting Information

The Supporting Information is available free of charge at https://pubs.acs.org/doi/10.1021/acs.jpcc.4c07330.

AFM data of laser-assisted ALEt under pure Ar flow and Cl_2/Ar flow (Figure S1); the time-resolved spectroscopy data during the laser excitation of Cl_2 molecules (Figure S2); the variables used in the laser dissociation of chlorine simulation (eqs S1−S3); the chlorine kinetics simulation setup (Figure S3); (a) spatial distribution of laser peak irradiance; (b) temporal profile of laser irradiance at the focal point (Figure S4); the detailed parameters used in the simulation (Table S1) (PDF)

■ AUTHOR INFORMATION

Corresponding Author

Costas P. Grigoropoulos − *Laser Thermal Laboratory, Department of Mechanical Engineering, University of California, Berkeley, California 94720, United States;* orcid.org/0000-0002-8505-4037; Email: cgrigoro@berkeley.edu

Authors

Runxuan Li − *Laser Thermal Laboratory, Department of Mechanical Engineering, University of California, Berkeley, California 94720, United States*

Matthew H. Eliceiri − *Laser Thermal Laboratory, Department of Mechanical Engineering, University of California, Berkeley, California 94720, United States*

Jingang Li − *Laser Thermal Laboratory, Department of Mechanical Engineering, University of California, Berkeley, California 94720, United States;* orcid.org/0000-0003-0827-9758

https://doi.org/10.1021/acs.jpcc.4c07330
J. Phys. Chem. C 2025, 129, 2460−2466

Vasileios Korakis − *Laser Thermal Laboratory, Department of Mechanical Engineering, University of California, Berkeley, California 94720, United States*

Rundi Yang − *Laser Thermal Laboratory, Department of Mechanical Engineering, University of California, Berkeley, California 94720, United States;* orcid.org/0000-0002-2877-939X

Yoonsoo Rho − *Department of Mechanical Engineering, Ulsan National Institute of Science and Technology, Ulsan 44919, Republic of Korea*

Brian W. Blankenship − *Laser Thermal Laboratory, Department of Mechanical Engineering, University of California, Berkeley, California 94720, United States;* orcid.org/0000-0003-4212-6835

Complete contact information is available at: https://pubs.acs.org/10.1021/acs.jpcc.4c07330

Notes

The authors declare no competing financial interest.

■ ACKNOWLEDGMENTS

Financial support awarded to the University of California, Berkeley, by the National Science Foundation through Grant CMMI-2024391 is gratefully acknowledged. The atomic layer etching experiments were conducted at the Laser Assisted Chemical Vapor Deposition (LACVD) apparatus at the UC Berkeley Marvell Nanofabrication Laboratory. The authors thank Sam Tsitrin and Dr. Andrew Dopilka for their assistance with experiment setup and sample characterizations. B.W.B. received support from the NSF Graduate Research Fellowship (DGE 2146752).

■ REFERENCES

(1) Moore, G. E. Cramming more components onto integrated circuits, Reprinted from Electronics, volume 38, number 8, April 19, 1965, pp.114 ff. *IEEE Solid-State Circuits Soc. Newsl.* **2006**, *11* (3), 33−35.

(2) Oehrlein, G. S.; Brandstadter, S. M.; Bruce, R. L.; Chang, J. P.; DeMott, J. C.; Donnelly, V. M.; Dussart, R.; Fischer, A.; Gottscho, R. A.; Hamaguchi, S.; et al. Future of plasma etching for microelectronics: Challenges and opportunities. *J. Vac. Sci. Technol. B* **2024**, *42* (4), 041501.

(3) Kanarik, K. J.; Lill, T.; Hudson, E. A.; Sriraman, S.; Tan, S.; Marks, J.; Vahedi, V.; Gottscho, R. A. Overview of atomic layer etching in the semiconductor industry. *J. Vac. Sci. Technol. A* **2015**, *33* (2), 020802.

(4) Gao, Q.; Cheng, C. C.; Chen, P. J.; Choyke, W. J.; Yates, J. T. Chlorine bonding sites and bonding configurations on Si(100)−(2 × 1). *J. Chem. Phys.* **1993**, *98*, 8308−8323.

(5) Nakane, K.; Vervuurt, R. H. J.; Tsutsumi, T.; Kobayashi, N.; Hori, M. In Situ Monitoring of Surface Reactions during Atomic Layer Etching of Silicon Nitride Using Hydrogen Plasma and Fluorine Radicals. *ACS Appl. Mater. Interfaces* **2019**, *11*, 37263−37269.

(6) Rho, Y.; Lee, K.; Wang, L.; Ko, C.; Chen, Y.; Ci, P.; Pei, J.; Zettl, A.; Wu, J.; Grigoropoulos, C. P. A laser-assisted chlorination process for reversible writing of doping patterns in graphene. *Nat. Electron.* **2022**, *5*, 505−510.

(7) Eliceiri, M.; Rho, Y.; Li, R.; Grigoropoulos, C. P. Pulsed laser induced atomic layer etching of silicon. *J. Vac. Sci. Technol. A* **2023**, *41* (2), 022602.

(8) Iimori, T.; Hattori, K.; Shudo, K.; Iwaki, T.; Ueta, M.; Komori, F. Laser-induced mono-atomic-layer etching on Cl-adsorbed Si(111) surfaces. *Appl. Surf. Sci.* **1998**, *130*−*132*, 90−95.

(9) Ishii, M.; Meguro, T.; Sugano, T.; Gamo, K.; Aoyagi, Y. Surface reaction control in digital etching of GaAs by using a tunable UV laser system: reaction control mechanism in layer-by-layer etching. *Appl. Surf. Sci.* **1995**, *86*, 554−558.

(10) Dubowski, J. J.; Compaan, A.; Prasad, M. Laser-assisted dry etching ablation of InP. *Appl. Surf. Sci.* **1995**, *86*, 548−553.

(11) Li, R.; Blankenship, B. W.; Wu, J.; Rho, Y.; Li, J.; Grigoropoulos, C. P. Laser-aided processing and functionalization of 2D materials. *Appl. Phys. Lett.* **2024**, *125* (7), 070502.

(12) Huang, S.; Li, J.; Fang, J.; Ding, H.; Huang, W.; Zhao, X.; Zheng, Y. Self-Limiting Opto-Electrochemical Thinning of Transition-Metal Dichalcogenides. *ACS Appl. Mater. Interfaces* **2021**, *13*, 58966−58973.

(13) Zhang, X.; Ho, J. R.; Grigoropoulos, C. P. Ultra-shallow p +-junction formation in silicon by excimer laser doping: a heat and mass transfer perspective. *Int. J. Heat Mass Transfer.* **1996**, *39*, 3835−3844.

(14) Houle, F. A. Basic mechanisms in laser etching and deposition. *Appl. Phys. A: mater. Sci. Process* **1986**, *41*, 315−330.

(15) Kim, E.; Ko, C.; Kim, K.; Chen, Y.; Suh, J.; Ryu, S.-G.; Wu, K.; Meng, X.; Suslu, A.; Tongay, S. Site Selective Doping of Ultrathin Metal Dichalcogenides by Laser-Assisted Reaction. *Adv. Mater.* **2016**, *28*, 341−346.

(16) Mogyorósi, P.; Piglmayer, K.; Kullmer, R.; Bäuerle, D. Laser-induced chemical etching of silicon in chlorine atmosphere. *Appl. Phys. A: Mater. Sci. Process.* **1988**, *45*, 293−299.

(17) Eliceiri, M.; Grigoropoulos, C. P. Comparison of transient absorption of laser ablation plasma with fundamental plasma absorption relations. *Appl. Phys. A* **2021**, *127* (7), 507.

(18) Zhang, W.; Zhou, R.; Yang, P.; Liu, K.; Yan, J.; Gao, P.; Tang, Z.; Li, X.; Lu, Y.; Zeng, X. Determination of chlorine with radical emission using laser-induced breakdown spectroscopy coupled with partial least square regression. *Talanta* **2019**, *198*, 93−96.

(19) Li, J.; Yang, R.; Rho, Y.; Ci, P.; Eliceiri, M.; Park, H. K.; Wu, J.; Grigoropoulos, C. P. Ultrafast Optical Nanoscopy of Carrier Dynamics in Silicon Nanowires. *Nano Lett.* **2023**, *23*, 1445−1450.

(20) Hori, M. Radical-controlled plasma processes. *Rev. Mod. Plasma Phys.* **2022**, *6* (1), 36.

(21) Hubinger, S.; Nee, J. B. Absorption spectra of Cl2, Br2 and BrCl between 190 and 600 nm. *J. Photochem. Photobiol. A* **1995**, *86*, 1−7.

(22) Li, L.; Lipert, R. J.; Lobue, J.; Chupka, W. A.; Colson, S. D. Adiabatic dissociation of photoexcited chlorine molecules. *Chem. Phys. Lett.* **1988**, *151*, 335−339.

(23) Park, J.; Lee, Y.; Flynn, G. W. Tunable diode laser probe of chlorine atoms produced from the photodissociation of a number of molecular precursors. *Chem. Phys. Lett.* **1991**, *186*, 441−449.

(24) Wang, P.; Fang, F. Defect-Mediated Atomic Layer Etching Processes on Cl-Si(100): An Atomistic Insight. *J. Phys. Chem. C* **2023**, *127*, 21106−21113.

(25) Li, J.; Hao, Y.; Yang, J.; Zhou, C.; Mo, Y. Vibrational structure, spin-orbit splitting, and bond dissociation energy of Cl2+($\tilde{X}\Pi g2$) studied by zero kinetic energy photoelectron spectroscopy and ion-pair formation imaging method. *J. Chem. Phys.* **2007**, *127*, 104307.

(26) Johnsen, A. J.; Alekseyev, A. B.; Balint-Kurti, G. G.; Brouard, M.; Brown, A.; Buenker, R. J.; Campbell, E. K.; Kokh, D. B. A complete quantum mechanical study of chlorine photodissociation. *J. Chem. Phys.* **2012**, *136* (16), 164310.

(27) Booth, J. P.; Azamoum, Y.; Sirse, N.; Chabert, P. Absolute atomic chlorine densities in a Cl2 inductively coupled plasma determined by two-photon laser-induced fluorescence with a new calibration method. *J. Phys. D: Appl. Phys.* **2012**, *45*, 195201.

(28) Chang, L. C.; Su, T.-M. Chemiluminescence spectra of chlorine atom recombination reactions. In *The Pacific Rim Conference on Lasers and Electro-Optics, Technical Digest.*, Optica Publishing Group, 1995, P32.

(29) Song, T. T.; Su, T. M. Recombination Reactions of Atomic Chlorine in Compressed Gases. 2. Geminate and Nongeminate Recombinations and Photolysis Quantum Yields with Argon Pressure Up to 180 bar. *J. Phys. Chem.* **1996**, *100*, 13554−13560.

(30) Jacksier, T.; Barnes, R. M. Atomic Emission of Chlorine: Spectra from 200 to 900 nm by Sealed Inductively Coupled Plasma-Atomic Emission Spectroscopy. *Appl. Spectrosc.* **1994**, *48*, 382−386.

(31) Radziemski, L. J.; Kaufman, V. Wavelengths, energy levels, and analysis of the second spectrum of chlorine (Cl ii)*. *J. Opt. Soc. Am.* **1974**, *64*, 366−389.
(32) Mikhailenko, M. S.; Pestov, A. E.; Chkhalo, N. I.; Zorina, M. V.; Chernyshev, A. K.; Salashchenko, N. N.; Kuznetsov, I. I. Influence of ion-beam etching by Ar ions with an energy of 200−1000 eV on the roughness and sputtering yield of a single-crystal silicon surface. *Appl. Opt.* **2022**, *61*, 2825−2833.
(33) Kullmer, R.; Bäuerle, D. Laser-induced chemical etching of silicon in chlorine atmosphere. *Appl. Phys. A: mater. Sci. Process.* **1988**, *47*, 377−386.
(34) Vella, J. R.; Elgarhy, M. A. I.; Hao, Q.; Donnelly, V. M.; Graves, D. B. Reactor wall effects in Si−Cl2−Ar atomic layer etching. *J. Vac. Sci. Technol. A* **2024**, *42* (4), 042604.
(35) Lymberopoulos, D. P.; Economou, D. J. Two-dimensional simulation of polysilicon etching with chlorine in a high density plasma reactor. *IEEE Trans. Plasma Sci.* **1995**, *23*, 573−580.
(36) Kanarik, K. J.; Tan, S.; Gottscho, R. A. Atomic Layer Etching: Rethinking the Art of Etch. *J. Phys. Chem. Lett.* **2018**, *9*, 4814−4821.
(37) Blankenship, B. W.; Meier, T.; Arvin, S. L.; Li, J.; Seymour, N.; De La Torre, N.; Hsu, B.; Zhao, N.; Mavrikos, S.; Li, R. Nondestructive Imaging of Manufacturing Defects in Microarchitected Materials. *ACS Appl. Engin. Mater.* **2024**, *2*, 1737−1742.
(38) Blankenship, B. W.; Li, J.; Jones, Z.; Parashar, M.; Zhao, N.; Singh, H.; Li, R.; Arvin, S.; Sarkar, A.; Yang, R. Spatially Resolved Quantum Sensing with High-Density Bubble-Printed Nanodiamonds. *Nano Lett.* **2024**, *24*, 9711−9719.
(39) Li, J.; Yang, R.; Higashitarumizu, N.; Dai, S.; Wu, J.; Javey, A.; Grigoropoulos, C. P. Transient Nanoscopy of Exciton Dynamics in 2D Transition Metal Dichalcogenides. *Adv. Mater.* **2024**, *36* (21), No. e2311568.
(40) Vaquero-Stainer, A.; Yoshida, M.; Hylton, N. P.; Pusch, A.; Curtin, O.; Frogley, M.; Wilson, T.; Clarke, E.; Kennedy, K.; Ekins-Daukes, N. J.; et al. Semiconductor nanostructure quantum ratchet for high efficiency solar cells. *Commun. Phys.* **2018**, *1* (1), 7.
(41) Blankenship, B. W.; Li, R.; Guo, R.; Zhao, N.; Shin, J.; Yang, R.; Ko, S. H.; Wu, J.; Rho, Y.; Grigoropoulos, C. Photothermally Activated Artificial Neuromorphic Synapses. *Nano Lett.* **2023**, *23*, 9020−9025.
(42) Zhang, Z.; Huang, Z.; Li, J.; Wang, D.; Lin, Y.; Yang, X.; Liu, H.; Liu, S.; Wang, Y.; Li, B. Endoepitaxial growth of monolayer mosaic heterostructures. *Nat. Nanotechnol.* **2022**, *17*, 493−499.

https://doi.org/10.1021/acs.jpcc.4c07330
J. Phys. Chem. C 2025, 129, 2460−2466